AIAA JOURNAL
Vol. 46, No. 10, October 2008

Kinetic Ignition Enhancement of Diffusion Flames by Nonequilibrium Magnetic Gliding Arc Plasma

Timothy Ombrello* and Yiguang Ju†
Princeton University, Princeton, New Jersey 08544
and
Alexander Fridman‡
Drexel University, Philadelphia, Pennsylvania 19104

DOI: 10.2514/1.33005

Kinetic ignition enhancement of CH_4–air and H_2–air diffusion flames by a nonequilibrium plasma discharge of air was studied experimentally and numerically through the development of a well-defined counterflow system. Measurements of ignition temperatures and major species, as well as computations of rates of production and sensitivity analyses, were performed to understand the kinetic enhancement pathways for ignition by plasma discharge of air. It was found that plasma discharge of air led to significant kinetic ignition enhancement illustrated by large decreases in the ignition temperatures for a broad range of strain rates. Examination of the radical and NO_x production in the plasma showed that the enhancement was caused primarily by the catalytic effect of NO_x. The results of numerical simulations of the counterflow burner with preheated air and NO_x addition showed the existence of different ignition regimes, which appeared due to the competition between radical production by NO_x and other pathways, as well as heat release. There were two ignition regimes for small concentrations of NO_x and three ignition regimes for large concentrations of NO_x. Numerical simulations agreed well with the experimental measurements and suggested a new strategy for plasma-assisted ignition in supersonic flow, where a combination of thermal and nonthermal plasma would work more efficiently for ignition enhancement.

I. Introduction

THE development of hypersonic airbreathing propulsion systems using hydrocarbon-based fuels has evoked many fundamental problems associated with combustion in supersonic flows. One of the major difficulties encountered has come from the flow residence times being of the same order of magnitude as the ignition delay and complete reaction times within the supersonic combustor. Therefore, the total heat release, thrust, and propulsive efficiency cannot fully be realized. One solution to this predicament is rooted in the fundamental problem of how to accelerate the ignition process in a combustion system. Furthermore, because some fuels (hydrocarbons) react more slowly than other fuels (hydrogen), and because hydrocarbon fuels have energy densities which are several times larger than hydrogen, the need for the development of new methods to accelerate ignition becomes particularly important.

It is well known that there are two main methods of accelerating an ignition process: thermally or kinetically. Thermal enhancement is accomplished by increasing the translational gas temperature to increase the reaction rates by the temperature-sensitive Arrhenius dependence. Kinetic enhancement is accomplished by decreasing the activation energies needed in the combustion system. By directly adding key intermediate species, radicals, ions, electrons, and excited species to the reacting system, the slow initiation or branching reactions are accelerated and/or bypassed.

Plasma has been investigated as an attractive means of accelerating ignition because it can be a source of elevated temperatures, radicals, ions, electrons, and excited species to thermally and/or kinetically enhance ignition. Plasma-assisted combustion has been extensively investigated since its inception in the early 19th century when the effect of an electric field on transport and diffusion in flames was examined [1]. More recently, in the 1980s, research on plasma-assisted combustion reemerged and focused on ignition enhancement and flame stabilization in supersonic flow [2–4]. Since then, many different types of plasma-enhancing applications have been developed and include plasma jets/torches [5], microwave discharges [6,7], radio frequency discharges [8], nanosecond pulsed discharges [9–11], dielectric barrier discharges [12], gliding arc discharges [13], and many others. Significant enhancement was observed in many of the developed plasma-flame systems with decreased ignition temperatures, showing clearly that plasma enhanced ignition. Unfortunately, the mechanisms of enhancement remained largely unknown, and much of the experimental data could not be explained completely. Because much of the past research was focused on developing plasma-flame systems for optimum enhancement in specific geometries, many contained complex and highly coupled hydrodynamic and reactive flows. The complicated flows and interactions created difficulties in decoupling the systems to pinpoint the exact mechanisms of enhancement. Because plasma has the ability to enhance combustion systems both thermally and kinetically, an isolation of the individual effects on ignition by decoupling the plasma-flame systems needed to be developed to identify the kinetic enhancement pathways.

In our previous study of plasma-assisted combustion using a well-defined platform of a counterflow diffusion flame integrated with the magnetic gliding arc (MGA), it was found that the strain rates at extinction were significantly increased with plasma discharge of the airstream [13]. However, the comparison of planar Rayleigh scattering and OH planar laser-induced fluorescence measurements with numerical simulations showed that the enhancement was predominately thermal due to the rapid recombination of active species at the lower air temperatures. Furthermore, because large concentrations of radicals existed in the flame, the smaller concentrations of plasma-produced radicals did not affect the

Presented as Paper 1025 at the 45th AIAA Aerospace Sciences Meeting and Exhibit, Reno, Nevada, 8–11 January 2007; received 22 June 2007; accepted for publication 30 April 2008.

*Graduate Student, Department of Mechanical and Aerospace Engineering, Engineering Quadrangle on Olden Street. Student Member AIAA.

†Associate Professor, Department of Mechanical and Aerospace Engineering, Engineering Quadrangle on Olden Street. Associate Fellow AIAA.

‡Professor, Drexel Plasma Institute, 34th and Lancaster Avenue. Associate Fellow AIAA.

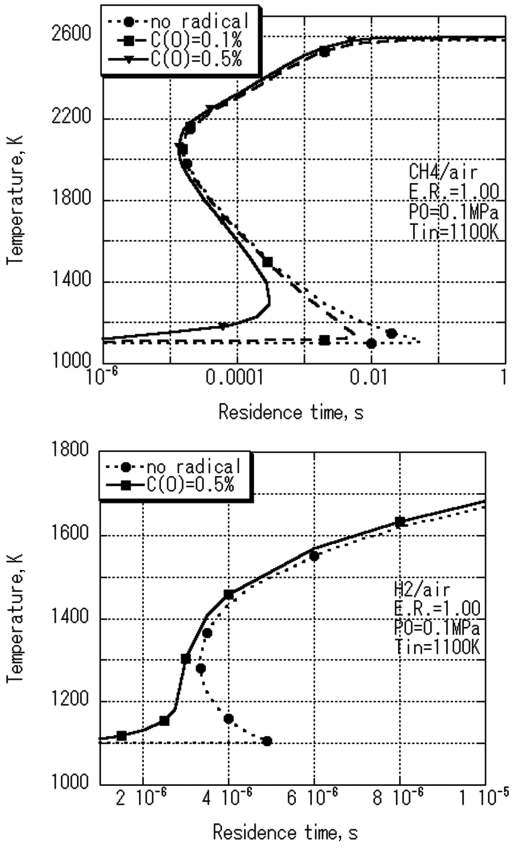

Fig. 1 Effect of radical addition on S curves of CH_4–air and H_2–air with $T_{in} = 1100$ K [14].

extinction limits. In addition to these findings, the numerical simulations of Takita and Ju [14] showed that, even though radical addition extended the extinction limits to higher strain rates, at low temperatures, the effect was significantly smaller than the enhancement by radicals on the ignition limit (Fig. 1). The results of our past work, as well as the work of Takita and Ju, showed that, to observe a kinetic effect of plasma on a combustion system, ignition phenomena needed to be considered.

When investigating the effects of plasma on a combustion system, both thermal and kinetic enhancing methods for ignition have been well studied, but a clear understanding of kinetic mechanisms from plasma-produced species were unknown. Therefore, the kinetic interaction of plasmas and flames needed to be studied in detail to understand the mechanisms of enhancement. The development of a well-defined plasma-flame ignition apparatus to isolate and study kinetic ignition enhancement was warranted and was the primary motivation for the present study. Detailed experimental and computational studies of plasma-enhanced ignition were performed through the integration of a nonequilibrium MGA plasma discharge with a counterflow CH_4–air and H_2–air diffusion flame burner to decouple the complex plasma-flame interaction and isolate fully the kinetic ignition enhancement mechanisms.

II. Experimental Apparatus

A. Nonequilibrium Magnetic Gliding Arc

The MGA is a nonequilibrium gliding arc that was developed in previous experiments of plasma-assisted flame stabilization [13]. For brevity, only an overview of the gliding arc system is discussed here. The MGA is a special type of gliding arc discharge that uses the Lorentz force created by current flowing within a magnetic field to rotate and stabilize the arc. The gliding arc is similar to a Jacob's ladder, where a potential is placed across two diverging electrodes and an arc is initiated at the smallest gap. The arc elongates as it glides along the electrodes, with the translational temperature of the arc continually decreasing and the temperature of electrons increasing,

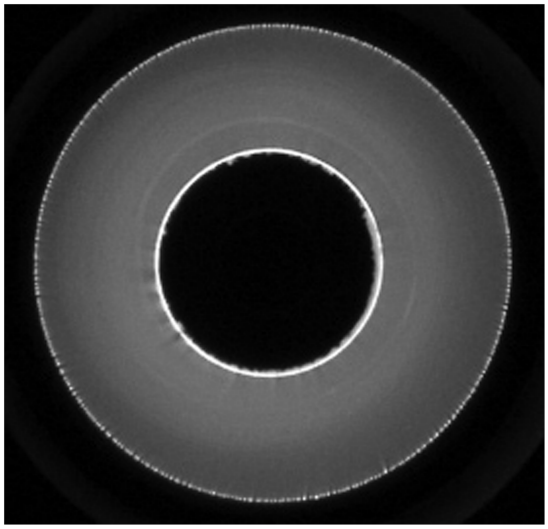

Fig. 2 Time-integrated top view of MGA, creating a plasma disk.

having less thermal dissociation and ionization and more direct electron impact dissociation and ionization to maintain the discharge. The electrons gain more energy, are accelerated by the electric field, and allow for the arc to have more nonequilibrium properties. In a Jacob's ladder, the arc only remains in the nonequilibrium regime for a short period of time before further elongation causes arc extinction. In the current study, to overcome the short nonequilibrium plasma lifetime, the diverging electrodes were placed in a helical geometry within a permanent magnetic field. Therefore, when the arc reached the largest gap in the system, it was stabilized in the near-extinction regime for an indefinite length of time because less energy was required to maintain the arc at that location than to reinitiate at the smallest gap [15]. The continual rotation of the arc at the largest gap produced a quasi-steady "plasma disk." A top view of the plasma disk is shown in Fig. 2 with an outer diameter of 38 mm and an inner diameter of 16 mm. The plasma disk was an intermediate translational temperature arc with thermal dissociation and ionization, as well as direct electron impact dissociation and ionization to maintain the discharge. The MGA was therefore in thermal nonequilibrium with the mean electron temperature (∼1.2–4 eV) about 10 times greater than the translational temperature (∼2500 K) [16].

B. Integration of Magnetic Gliding Arc with Counterflow Diffusion Flame Burner

The MGA device was integrated with a combustion system to provide a simplified platform to study the kinetic effects of the nonequilibrium plasma-flame interaction. Previous work by the authors' group included integration of the MGA with a counterflow diffusion flame burner for flame stabilization experiments [13]. The same basic design was again chosen for the ignition work because of its proven validation with the past experiments. Additionally, to directly compare the plasma-assisted ignition with preheated air ignition, the counterflow system was augmented to include an electric heater to raise the air temperature to the ignition temperature of CH_4–air and H_2–air diffusion flames. The electric heater and the heated nozzle or plasma system were placed in series to provide a comparison between preheated-air-only ignition and plasma-assisted ignition. The counterflow burner was chosen because it is a well-established system that could provide four key benefits: minimal buoyancy effects, simplified flame geometry, the ability to define a flow velocity gradient (strain rate or inverse of residence time) on the centerline near the stagnation plane of the two impinging jets, and, lastly, geometry that allows for proven comparisons to computational simulations.

For all experiments, the upper nozzle of the counterflow system consisted of a water-cooled 15 mm inner diameter nozzle with a nitrogen coflow to isolate the jet from any ambient effects. The fuel

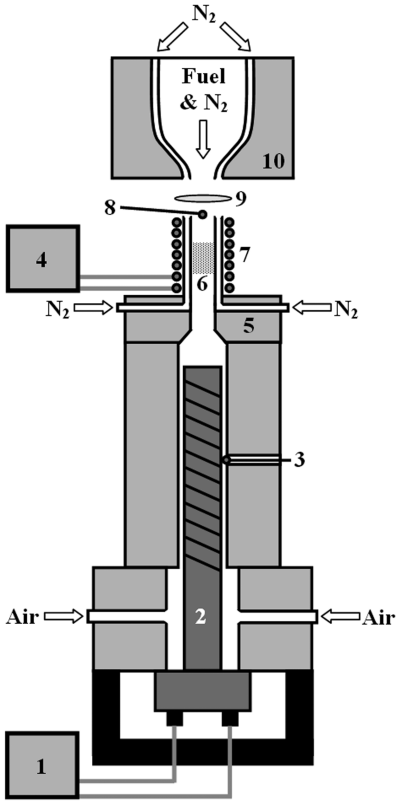

Fig. 3 Heated nozzle counterflow ignition apparatus: 1) silicon controlled rectifier, 2) silicon carbide heater, 3) *R*-type thermocouple, 4) Variac, 5) heated nozzle, 6) flow straightening ceramic honeycomb, 7) Kanthal wire heated quartz nozzle, 8) *K*-type thermocouple, 9) diffusion flame, 10) water-cooled nozzle with N_2 coflow.

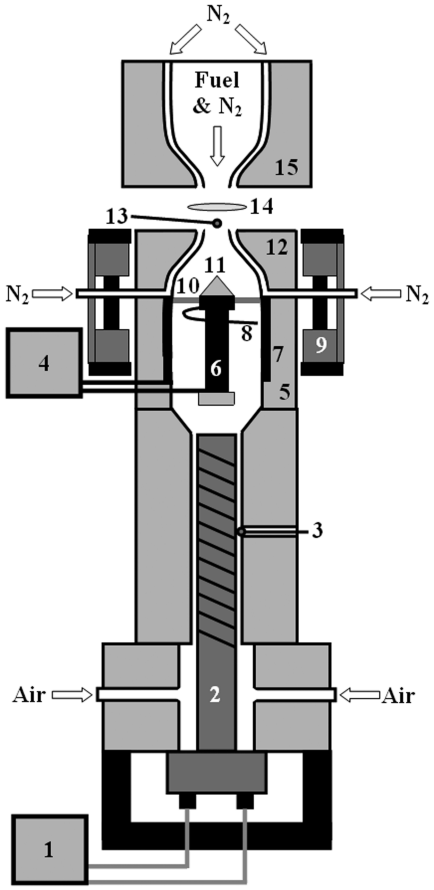

Fig. 4 MGA counterflow ignition apparatus: 1) silicon controlled rectifier, 2) silicon carbide heater, 3) *R*-type thermocouple, 4) MGA plasma power supply, 5) MGA device, 6) cathode, 7) anode, 8) gliding arc initiation wire, 9) magnets, 10) MGA, 11) insulator, 12) nozzle with N_2 coflow, 13) *K*-type thermocouple, 14) diffusion flame, 15) water-cooled nozzle with N_2 coflow.

used (CH_4 or H_2) was passed through the upper nozzle and was diluted in 80% N_2 to weaken the strength of the flame. The lower nozzle of the counterflow system consisted of both a preheating system as well as either the heated nozzle or the MGA device. The preheating system was housed in high-temperature silica ceramic and contained a silicon carbide heater that was capable of raising the temperature of the air in excess of 1600 K. A thermocouple was placed approximately 1 mm from the surface of the heater and was used as a feedback sensor to the heater's power supply to maintain the desired temperatures.

There were two different lower nozzles: the heated nozzle and the MGA device. The heated nozzle attachment was used for preheated-air-only ignition and consisted of a 15 mm inner diameter quartz tube with a nitrogen coflow. A schematic of the system is shown in Fig. 3. To minimize heat loss, Kanthal heater wire was wrapped around the outside of the quartz tube with a variable ac power supply for its energy requirements. The MGA device attachment was used to activate the preheated air by the plasma discharge for ignition. The MGA assembly consisted of high-temperature cast silica ceramic to hold the stainless steel electrodes in place. Permanent neodymium magnets were located radially around the outside diameter of the outer electrode of the MGA device and were used to create the magnetic field and rotate the arc. The magnets were not adjacent to the outer electrodes to minimize heat loss and maintain the magnets well below their demagnetizing temperature. A 42-mm-long nozzle with an exit diameter of 15 mm was placed downstream of the MGA device to establish the lower nozzle of the counterflow burner. A schematic of the system is shown in Fig. 4.

C. Ignition Temperature Measurements

Measurements were made of the ignition temperatures on the counterflow apparatus using both the heated nozzle and the MGA device. The convertible counterflow system was ideal for a comparison of the ignition temperatures with and without plasma activation of the preheated air for the same flow conditions. Using the heated nozzle, the flow was initially fixed through the system (20% CH_4 or 20% H_2 in 80% N_2 vs air) and the power was supplied to the silicon carbide heater and Kanthal wire heater to raise the temperature of the air to within 50 K of the ignition temperature of the given combustible flow. A steady-state temperature was established by allowing the system to run at the same heater power and air flow rate for about an hour. The flow was then ignited with an external source to allow for visualization and adjustments to optimize the alignment and flow in the system. Temperature profile measurements across the exit of the lower nozzle and between the lower nozzle and the stagnation plane were taken to ensure that the temperature was peaked along the axis at the exit of the lower nozzle. A *K*-type thermocouple was used to measure the ignition temperature because it did not suffer from any catalytic surface effects. Care was taken to ensure that the same location in the flow was always measured. Temperature measurements were consistently made axially at the exit of the lower nozzle. Because the thermocouple disrupted the flow, allowing for premature ignition, it was placed on a translation apparatus that could repeatedly and consistently move the thermocouple from a location outside of the flow to the same axial location at the exit of the lower nozzle.

To achieve ignition, the temperature of the air was raised slowly in small increments (by approximately 2–3 K close to the ignition temperature) until ignition was achieved by increasing the power supplied to the silicon carbide heater. The heater power at which ignition occurred was recorded and the flame extinguished by closing off the supply of fuel. The heater power was then lowered, the fuel turned on, and the flowfield was correctly adjusted and optimized. The heater power was again increased, ignition achieved,

and power recorded. Once the power at ignition was found to be consistently the same several times, the fuel supply was closed off and the heater adjusted to that power. The thermocouple was placed in the flow axially at the exit of the lower nozzle and the temperature measured. The measured temperature was defined as the ignition temperature. The procedure to find the ignition temperature was completed at least 10 separate times to establish repeatability. Furthermore, for radiation corrections to be performed a posteriori, the temperatures of the parts of the apparatus in line of sight and in close proximity to the thermocouple were measured.

A similar procedure was followed for measuring the ignition temperatures when using the MGA device. In addition to the temperature being raised to within 50 K of ignition by the silicon carbide heater, the plasma power supply was adjusted to a fixed power and the system was allowed to reach a steady-state temperature. The same procedure as that of the heated nozzle was followed to find the ignition temperatures for plasma activation of the air. Furthermore, special care was taken to ensure that the MGA did not become unstable and produce any high-temperature regions that would convect downstream with the flow and lead to localized ignition. The localized ignition would yield false underestimates of the actual ignition temperatures.

Most importantly, any difference in the measured ignition temperatures between the heated nozzle and MGA device would be kinetic because of the minimization of all localized thermal effects. The experiment therefore provided a well-defined system to study kinetic ignition enhancement by a nonequilibrium plasma.

III. Results

A. Experimental Ignition Temperature Results

Measurements were taken of the ignition temperatures using both the heated nozzle and MGA attachment to the counterflow diffusion flame burner for a strain rate range of 200–350 s^{-1} for CH_4 and 150–350 s^{-1} for H_2. For the MGA, the current was fixed at 350 mA for CH_4 and 140 mA for H_2, with powers of 250 and 130 W, respectively. The results of the ignition temperatures for CH_4 are shown in Fig. 5 and for H_2 in Fig. 6. The plotted data points were averages from over 10 measurements which never deviated by more than several percent, establishing excellent repeatability. For both fuels, there was a significant decrease in the ignition temperature when using the MGA, with up to a 167 K decrease for CH_4 and up to 74 K for H_2. The decreased ignition temperature results (and hence decreased ignition delay times) at the same strain rates and fuel concentrations showed clearly that there was a significant kinetic effect of the MGA on the ignition of CH_4–air and H_2–air counterflow diffusion flames. To gain insight into the mechanisms of the kinetic enhancement, numerical simulations were performed.

B. Numerical Simulations of Ignition of Counterflow Diffusion Flames

Numerical simulations were implemented to validate and explain the interaction of the MGA with the ignition of the counterflow diffusion flames. The code used was from one of the authors' previously developed code for counterflow flame simulations [18]. With the given geometry of the counterflow burner, simulations using detailed chemistry [both GRI-2.11 [19] and GRI-3.0 [20] for CH_4, and Li et al. [21] (H_2) with Mueller et al. [22] (NO_x) for H_2] were performed. The maximum (flame) temperature versus strain rate S curve was computed and the ignition temperatures were found as a function of strain rate.

1. *Ignition with Preheated Air Only*

The S-curve responses were obtained for preheated air only as a function of air temperature for both CH_4 and H_2. The curves for CH_4 are shown in Fig. 7. Because of the difficulty in observing the first ignition limit in the temperature coordinate, the maximum hydrogen radical concentration curve is shown as an analogous curve for 1200 K. It is noted that the local extremum of the maximum temperature and hydrogen radical concentration occurred at the same strain rate. The ignition-extinction S curves using GRI-3.0 exhibited two ignition and two extinction limits. The dual ignition limits for CH_4–air ignition have been observed in past work [23] and are strongly dependent on the reaction rate of $CH_3 + HO_2 \Leftrightarrow CH_3O + OH$. The lower temperature/strain rate ignition limits (the first ignition limit) had a maximum temperature in the flowfield that was equal to the air temperature, indicating that thermal feedback was negligible for ignition. However, for the higher temperature/

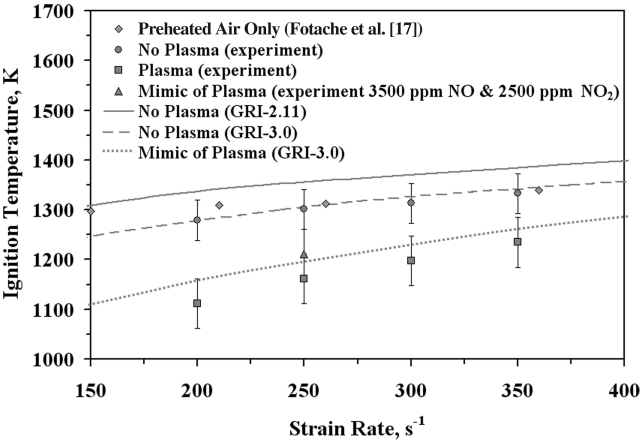

Fig. 5 Comparison of experimental and computational results of ignition temperatures with 20% CH_4 in N_2 vs air for preheated air and MGA ($I = 350$ mA) for $a = 200$–350 s^{-1}.

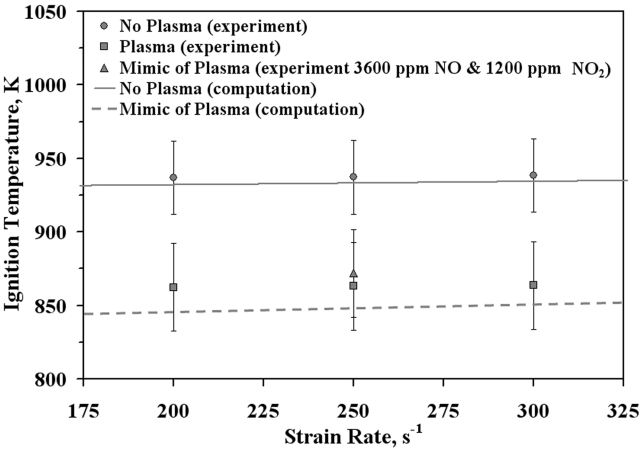

Fig. 6 Comparison of experimental and computational results of ignition temperatures with 20% H_2 in N_2 vs air for preheated air and MGA ($I = 140$ mA) for $a = 200$–350 s^{-1}.

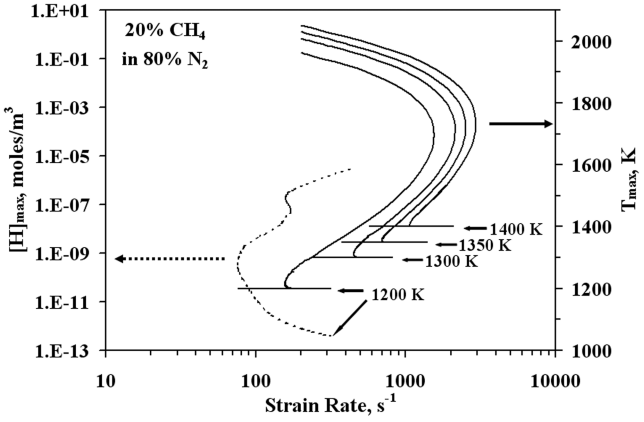

Fig. 7 S-curve response for 20% CH_4 in N_2 vs heated air as a function of maximum temperature and atomic hydrogen concentration for various strain rates using GRI-3.0.

strain rate ignition limit (the second ignition limit), there was a considerable temperature increase. Therefore, thermal runaway was needed to accelerate ignition at this limit. The *S*-curve responses using GRI-2.11 did not exhibit the dual limit behavior, giving slightly different temperature and strain rate results for the ignition limits. Therefore, both GRI-3.0 and GRI-2.11 were used for comparison to experimental results.

2. Ignition Enhancement by Magnetic Gliding Arc

The MGA produced radicals, ions, electrons, and excited species that had the potential to create new pathways for fuel oxidation and to accelerate ignition processes. A simplified approach was taken first to gain insight into the mechanisms of the observed ignition enhancement. Because ion recombination was assumed to be much faster than the flow residence time, radicals and nonexcited species were only considered in the computational models. Therefore, the plasma-produced species could be modeled with traditional detailed combustion mechanisms. Furthermore, because the MGA was activating dry air, there would only be oxygen- and nitrogen-containing species. Optical emission spectroscopy was performed on the MGA and the measurements taken were used to compute the reduced electric field and electron temperature. The electric field data and the electron temperature computed from the Boltzmann equation for electrons in weakly ionized gases were used to predict the species produced by the plasma discharge [24]. The main species that were found to exist and were expected to affect the ignition process of the system included O and NO_x. Atomic oxygen and NO_x were therefore used as boundary conditions on the air side of the counterflow simulation to mimic the MGA produced species and explain the enhancement. The temperature versus strain rate *S* curves were calculated for various initial temperatures and strain rates to obtain the ignition temperatures. Numerical results showed that the effect of even up to 1000 ppm of O at the air side boundary yielded negligible enhancement, even when combined with NO_x addition. The rapid recombination, and hence temperature increase, during transport between the nozzle exit and reaction zone was the cause of the negligible enhancement. Because 1000 ppm of O was well above what was expected at the exit of the nozzle, one can reasonably conclude that the effect of O was negligible. Furthermore, there was no appreciable difference in the experimentally measured temperature profiles between the nozzle exit and stagnation plane for both the heated nozzle and MGA, indicating that the temperature increase due to O recombination between the nozzle exit and the reaction zone was also negligible. The only species that remained were NO_x ($\sim$5000 ppm), which were the primary species used in the computational simulations.

To confirm that the predicted concentration of NO_x produced by the MGA was actually present, NO_x measurements were conducted by using a chemiluminescent NO_x analyzer (California Analytical Instruments, Model 300-CLD) and later confirmed using Fourier transform infrared spectroscopy (FT-IR) (Nicolet Magna-IR 5500). The chemiluminescent NO_x analyzer and FT-IR were calibrated with known concentrations of NO and NO_2, and then used to measure the NO_x concentrations axially at the exit of the lower nozzle for the same conditions as when the ignition temperatures were measured. The measured NO_x concentrations averaged 6000 ppm for the CH_4 ignition conditions and 4000 ppm for the H_2 ignition conditions, which were within good agreement with the estimated plasma production of NO_x. For simplicity of calculations, all of the NO_x at the boundary was assumed to be NO only. Because the enhancement of ignition from NO was much more significant than from NO_2, the input of only NO would yield an overestimate of the ignition enhancement compared with the experimental results.

It was of interest to note that the MGA was an efficient producer of NO_x by nonequilibrium processes in the plasma arc. The MGA had a translational gas temperature of approximately 2500 K and the flow had residence times through the arc on the order of 10 ms. Calculations using a thermal NO_x mechanism far underestimated concentrations of NO_x that were measured experimentally [24]. Therefore, nonequilibrium processes, such as direct electron impact dissociation reactions of

$$N_2 + e \rightarrow N + N + e \quad (1)$$

$$O_2 + e \rightarrow O + O + e \quad (2)$$

significantly contributed to the NO_x mechanism by providing the larger concentrations of atomic nitrogen and oxygen for NO production by the reactions

$$N + O_2 \rightarrow NO + O \quad (3)$$

$$N_2 + O \rightarrow NO + N \quad (4)$$

C. Comparison of Experimental and Computational Results

The computational results of ignition with heated air and the MGA were compared with the experimental results and are shown in Fig. 5 and 6 for CH_4 and H_2, respectively. There could be a direct comparison of the experimental and numerical results because the temperature increments used in the experiments to achieve ignition were small (on the order of 2–3 K), approximating steady-state ignition. Therefore, the temperatures measured could be compared with the steady-state solutions found in the numerical simulations. For the case of preheated air only (without plasma), the ignition temperatures from the preheated-air-only *S* curves of maximum temperature versus strain rate for CH_4 using GRI-3.0 were in good agreement with the experimental results, whereas GRI-2.11 gave an overestimate of the ignition temperature across the investigated range of strain rates. Furthermore, the H_2 mechanism (Li et al. [21]) with NO_x (Mueller et al. [22]) also gave good quantitative agreement with the experimental results. Therefore, the validated mechanisms of GRI-3.0 and Li's H_2 with Mueller's NO_x were used for the inclusion of plasma-produced NO to attempt to explain the MGA enhancement.

The maximum possible concentrations of NO measured for both cases of CH_4–air and H_2–air by the chemiluminescent NO_x analyzer and FT-IR spectrometer were used as initial inputs to the air side boundary of the counterflow simulation to mimic the MGA. For both the CH_4–air and H_2–air diffusion flames, the results from the computation agreed qualitatively with the experimental results, showing significantly decreased ignition temperatures. To confirm whether the primary species of ignition enhancement was NO_x, the air was seeded with the concentrations of NO_x measured axially at the exit of the lower nozzle and the ignition temperatures were again measured. The strain rate of 250 s^{-1} was chosen for both the CH_4 and H_2 flames because it was in the middle of the experimental range of strain rates. The results for both CH_4 and H_2 are also shown in Figs. 5 and 6. There was good agreement between the experimental results with plasma activation, the experimental results with NO_x addition, and the computational results. Furthermore, the experimental results with NO_x addition were slightly elevated above the computational results, reaffirming that NO affected ignition more than NO_2. Therefore, NO was the primary source of ignition enhancement by the plasma and the mechanisms were appropriately validated in the computations.

D. Kinetic Ignition Enhancement by NO_x and New Ignition Regimes

Both our experimental and numerical simulations showed that the ignition enhancement by the plasma was dominated by the significant concentrations of NO. Also, NO has been shown to enhance ignition in past work [25–27]. Therefore, further numerical simulations were performed to examine the effect of NO on ignition beyond the strain rates and temperatures than were attainable with the current experimental setup.

As shown in the experimental results, NO production by the plasma discharge led to lower ignition temperatures than those of preheated air only. To demonstrate the difference between ignition with and without the plasma discharge, the ignition temperatures versus strain rates were computed using GRI-3.0 with and without 10,000 ppm of NO addition and are shown in Fig. 8. For preheated

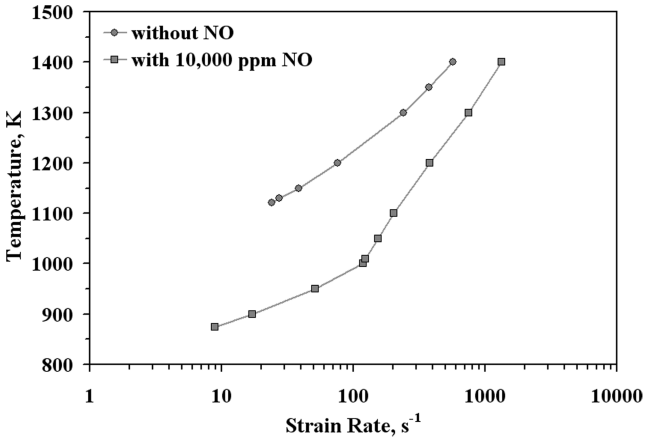

Fig. 8 Comparison of NO enhancement of ignition for different boundary temperatures.

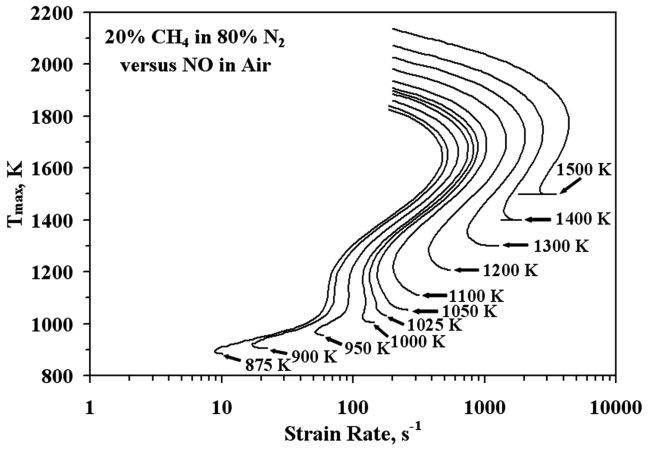

Fig. 9 *S*-curve response for 20% CH_4 in N_2 vs preheated air with 10,000 ppm NO as a function of maximum temperature and strain rate.

air, ignition could not occur below 1100 K, whereas with 10,000 ppm of NO, ignition occurred as low as 900 K. It was also found that, for the same temperature or same strain rate, ignition could occur, respectively, at much higher strain rates and at much lower temperatures with NO addition.

To examine the impact of NO production on ignition enhancement, the ignition *S* curves were calculated for NO addition at 100, 1000, 10,000, and 100,000 ppm, respectively. For an example, the ignition *S* curves for 10,000 ppm of NO addition are shown in Fig. 9. Starting at low ignition temperatures (hence lower strain rates), there existed one ignition limit, but around 950 K, a second ignition limit emerged.

To examine Fig. 9 in more depth, the relative maximum temperatures at which the ignition limits occurred were taken into account. According to the *S*-curve response, the lowest local minimum strain rate on each *S* curve corresponded to the actual ignition limit. Therefore, for each of the *S* curves in Fig. 9, there existed only one ignition limit which was used for comparison to the experimental results. To better understand this concept, the ignition limits from Fig. 9, with their associated boundary temperatures and maximum temperatures, were plotted in Fig. 10. Interestingly, there existed three distinctly different ignition regimes, denoted 1, 2, and 3, in Fig. 10. For low boundary temperatures, ignition regime 1, the maximum temperature between the two nozzles was close to the boundary temperature. However, for ignition regime 2, at temperatures between 1000 and 1300 K, the maximum temperature was significantly elevated above the boundary temperature. As the boundary temperature was increased to 1400 and 1500 K, ignition regime 3 had a maximum temperature equal to the boundary temperature.

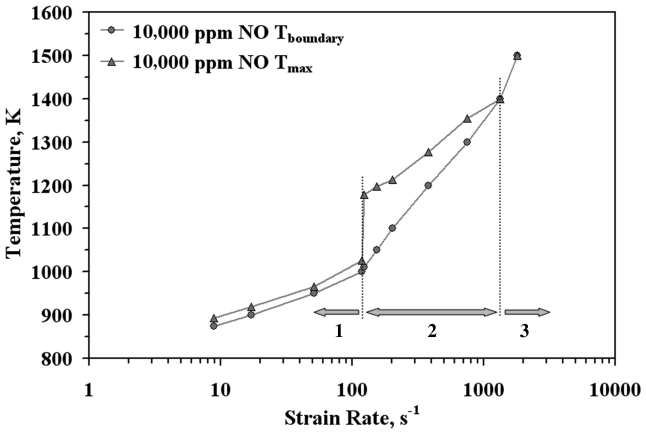

Fig. 10 Three ignition regimes from *S*-curve responses for 20% CH_4 in N_2 vs preheated air with 10,000 ppm NO.

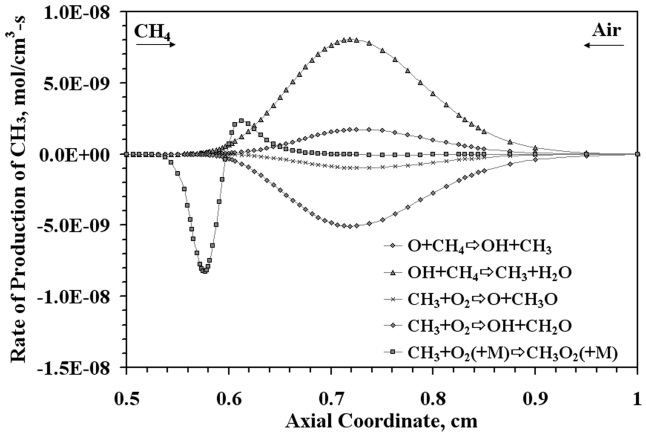

Fig. 11 Rate of production of CH_3 with $T_{boundary} = 1200$ K without NO.

E. Catalytic NO Effect for Radical Production

To identify the catalytic NO pathways for ignition enhancement and their dependence on air temperature, the rates of production of key species were found and sensitivity analyses were performed at the ignition limits to examine the most important reactions with the addition of NO. The rate of production of each species from each reaction was found for every reaction in the mechanism. This allowed for identification of the important pathways of production and consumption within the domain of the counterflow system, and to allow for a deeper understanding of the three ignition regimes identified in Fig. 10.

First, an understanding of how NO allowed for ignition at much lower temperatures than preheated air (Fig. 8) was sought. The rates of production of some of the key species for preheated air only and 1000 ppm of NO addition both at an air temperature of 1200 K for CH_4–air were calculated. For preheated air only, without NO addition, a rate of production analysis was performed and the results are shown in Fig. 11. At the ignition limit, the reaction

$$CH_3 + O_2(+M) \rightarrow CH_3O_2(+M) \quad (5)$$

was a sink for CH_3 radicals and was an effective termination reaction, because the only reaction for the consumption of CH_3O_2 was the reverse of reaction (5). It was produced upstream of the reaction zone on the fuel side, with the concentration equilibrating at a significant value. Therefore, the active CH_3 radical was consumed and taken out of the ignition process, significantly hindering ignition. Reaction (5) competed with the typical CH_3 consumption reactions of

$$CH_3 + O_2 \rightarrow O + CH_3O \quad (6)$$

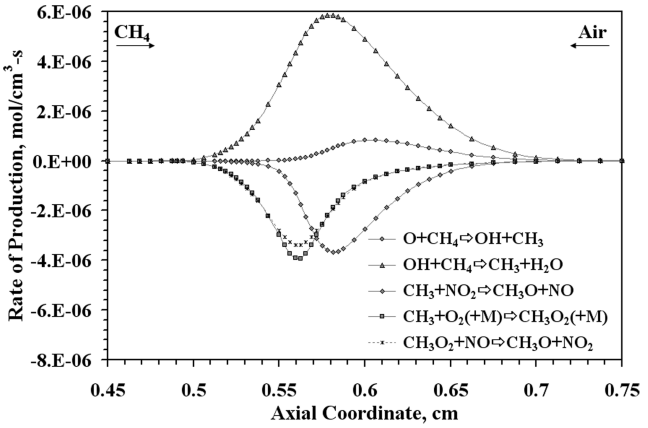

Fig. 12 Rate of production of CH_3 and CH_3O_2 with $T_{boundary} = 1200$ K with 1000 ppm of NO.

$$CH_3 + O_2 \rightarrow OH + CH_2O \quad (7)$$

$$CH_3 + HO_2 \rightarrow OH + CH_3O \quad (8)$$

$$CH_3 + CH_3(+M) \rightarrow C_2H_6(+M) \quad (9)$$

With the addition of NO, the ignition pathway changed significantly because reaction (5) was no longer a termination reaction because of the reaction

$$CH_3O_2 + NO \rightarrow CH_3O + NO_2 \quad (10)$$

Figure 12 confirms this, showing that there was a new pathway allowing for CH_3O_2 consumption, but also that there existed a catalytic cycle to replenish the NO in the system, while also producing more active radicals by the reaction

$$CH_3 + NO_2 \rightarrow CH_3O + NO \quad (11)$$

Therefore, CH_3O_2 became an active radical and there was a new pathway for CH_3 oxidation by NO. Another catalytic NO enhancement pathway that existed in the system to aid in the ignition process was from the reaction with the fairly inactive HO_2 radical via the reactions

$$HO_2 + NO \rightarrow OH + NO_2 \quad (12)$$

$$H + NO_2 \rightarrow OH + NO \quad (13)$$

The present results followed what was expected because reactions (10–13) are the four key reactions which lead to the catalytic NO effect for CH_4 ignition enhancement [25–27].

After identifying the key catalytic NO enhancement pathways, the three different ignition regimes shown in Fig. 10 were examined. Again, a rate of production analysis for some of the governing species for ignition was performed. The analysis was conducted at the three ignition temperatures of 900, 1015, and 1500 K, one in each ignition regime. The results in ignition regime 1 showed that the NO cycle catalyzed the inactive CH_3O_2 and HO_2 by reactions (10–13). The small difference between the maximum temperature and the boundary temperature was attributed to the exothermicity of the reactions involved in the catalytic NO cycles, which were identified in reactions (10–13). The enhancement pathways by NO produced a small amount of heat, only raising the maximum temperature on the order of 2%. Interestingly, if heat release was suppressed, the ignition limits could not be achieved. Instead, the mixture would not ignite, even at the lowest strain rate. The result indicated that, not only did the catalytic NO cycles raise the maximum temperature in the system, the slightly elevated temperatures were required for ignition.

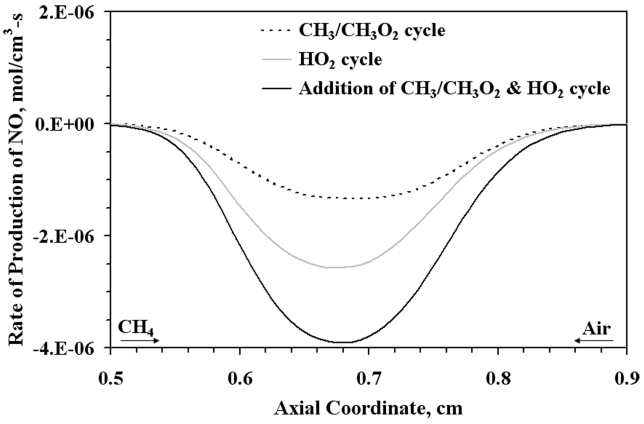

Fig. 13 Rate of production of NO with $T_{boundary} = 900$ K for both the CH_3/CH_3O_2 and HO_2 catalytic NO cycle with 10,000 ppm of NO.

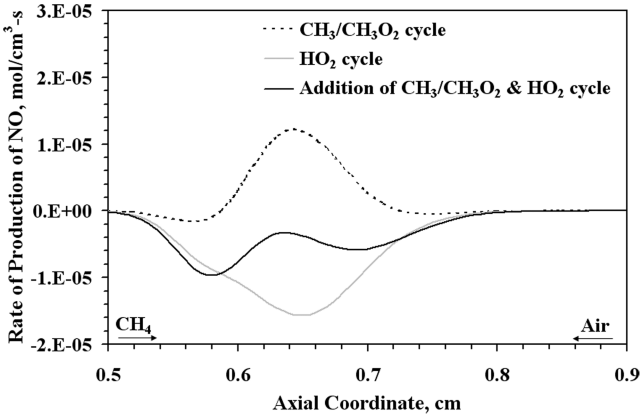

Fig. 14 Rate of production of NO with $T_{boundary} = 1015$ K for both the CH_3/CH_3O_2 and HO_2 catalytic NO cycle with 10,000 ppm of NO.

The catalytic cycle needed some thermal feedback to achieve ignition.

When the boundary temperature was increased to approximately 1000 K, the maximum temperature became elevated more than 15% higher than the boundary temperature. The maximum temperature rose above the boundary temperature and signified the transition to ignition regime 2. In this regime, much more thermal feedback was required as compared with ignition regime 1. There still existed significant ignition enhancement by NO addition, but the pathways for enhancement changed. To understand the new ignition pathways, a comparison of the catalytic NO cycles for 900 and 1015 K, respectively, for 10,000 ppm of NO addition through rate of production plots of NO are shown in Figs. 13 and 14. For a boundary temperature of 900 K (Fig. 13), the catalytic NO cycles with both CH_3/CH_3O_2 and HO_2 consumed the NO in the system to produce the active radicals needed for ignition. For 1015 K (Fig. 14), the HO_2 catalytic cycle still consumed the NO in the system, whereas the CH_3/CH_3O_2 catalytic cycle produced NO. The discrepancy came from the relative production and consumption of NO by reactions (10) and (11). Because there was a significant production of NO in the system by the CH_3/CH_3O_2 catalytic cycle, reaction (11) dominated over reaction (10). Furthermore, because the concentration of NO added to the system was identical for both 900 and 1015 K, reaction (10) would be affected by a deficiency of CH_3O_2. To confirm this, Fig. 15 showed that the rate of production of CH_3O_2 from CH_3 significantly decreased from 900 to 1015 K relative to the other CH_3 consumption reaction (11). Therefore, reaction (11) dominated the NO reactions involved in the ignition enhancement because there was less CH_3O_2 produced. To explain why there was such a large increase in the maximum temperature over the boundary temperature in ignition regime 2, the exothermicity of the catalytic

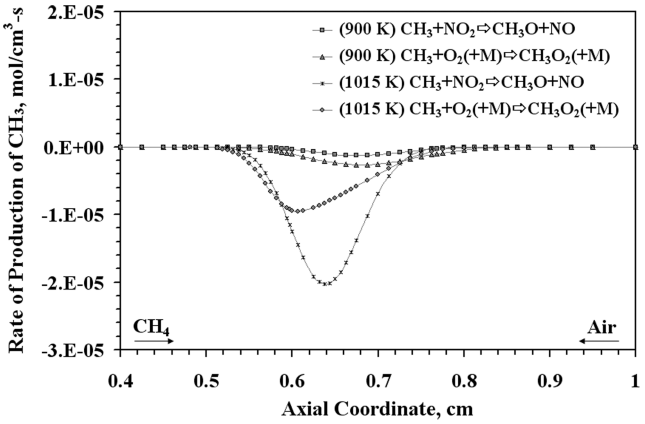

Fig. 15 Rate of production of NO with $T_{boundary} = 900$ and 1015 K showing decreased CH_3O_2 production with increased temperature with 10,000 ppm of NO.

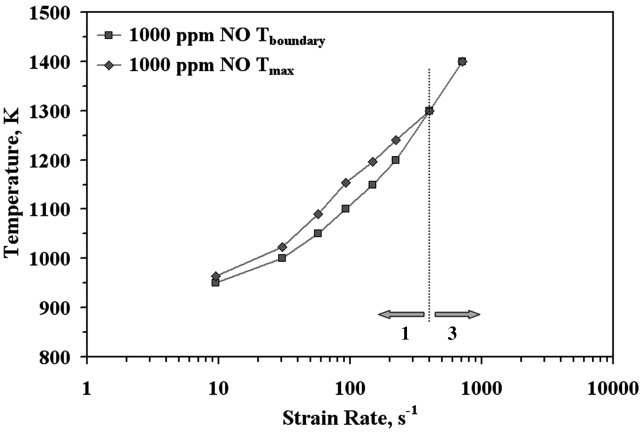

Fig. 16 Ignition regimes from *S*-curve responses for 20% CH_4 in N_2 vs preheated air with 1000 ppm NO.

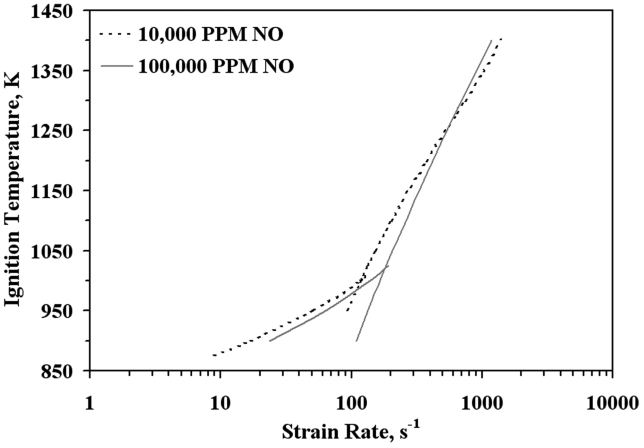

Fig. 17 Comparison of ignition temperature vs strain rate showing crossing point and hence critical NO concentrations of 10,000 and 100,000 ppm of NO.

NO cycles as well as the radical pool needed to be considered. First, reaction (11) dominated over reaction (10) for the consumption of CH_3 at 1015 K (Fig. 15) and because reaction (11) is more exothermic than reaction (10), there was much more heat production overall. Second, by having only a strong HO_2 catalytic NO cycle and a lack of a complete CH_3/CH_3O_2 catalytic cycle, the catalytic radical production was diminished. Reaction (11) acted only as another oxidation pathway for CH_3 because the NO_2 pool was not replenished for the catalytic cycle by reaction (10). Therefore, the HO_2 catalytic NO cycle and reaction (11) did not solely allow for the critical branching factor to be achieved for ignition. There needed to be some additional heat release to activate other CH_3 oxidation pathways such as reactions (6–8) to aid in the production of radicals. In the second ignition regime, the catalytic NO cycles were not the dominating pathways for radical production and ignition enhancement. The NO addition still produced active radicals, just less efficiently than at lower temperatures, hence the elevation of the maximum temperature far above the boundary temperature.

Toward the upper temperature range of ignition regime 2, even though there still existed a catalytic NO cycle to produce radicals needed for ignition, the boundary temperatures became sufficiently high, and other pathways were much faster and far more efficient at producing radicals. Therefore, around 1400 K, the third ignition regime emerged. The reaction rates of reactions (6–8) increased to a level where they could produce enough radicals to reach the critical branching factor with no thermal feedback.

Interestingly, the three ignition regimes observed for 10,000 ppm of NO addition were not present for all concentrations of NO addition. For example, with 1000 ppm of NO addition, a similar plot to Fig. 10 was made and is shown in Fig. 16. With 1000 ppm of NO addition, there existed only two ignition regimes. The two ignition regimes were similar to ignition regimes 1 and 3 shown in Fig. 10. At lower temperatures, the catalytic role of NO allowed for ignition at much lower temperatures than achievable with preheated air, and there was a small difference between the maximum temperature and boundary temperature in the system. With an increase in the boundary temperature and strain rate, the second ignition regime found for 10,000 ppm of NO was not present for 1000 ppm of NO. Instead, there was a direct transition from the first to the third ignition regime where the maximum temperature and boundary temperature were equal. This was due to the temperatures involved in the system. Because the ignition temperatures were much higher for 1000 ppm of NO (closer to the preheated air ignition because of less ignition enhancement) than for 10,000 ppm of NO, there was no intermediate region where the CH_3/CH_3O_2 catalytic cycle was suppressed because of the lack of CH_3O_2 and when the high-temperature CH_3 oxidation mechanisms dominated. Therefore, there was a smooth transition between ignition regimes 1 and 3 because of the higher temperatures supporting the typical CH_3 oxidation pathways when the CH_3O_2 radical pool began to diminish. If a level of NO addition between 1000 and 10,000 ppm of NO were chosen, there would be a slow transition to a second ignition regime which was shown for 10,000 ppm of NO.

Lastly, if a sufficiently large concentration of NO was added to the system, there existed a critical concentration at which ignition was inhibited at high temperatures and strain rates. An example of this is shown in Fig. 17 with the crossing of the ignition curves with different concentrations of NO. A sensitivity analysis was performed at the ignition limits at 1400 K for 10,000 and 100,000 ppm of NO addition after the crossover in Fig. 17. The sensitivity coefficient was defined as

$$\text{sensitivity coefficient} = \frac{\partial \ln(a_{\text{ignition}})}{\partial \ln(k_i)} \tag{14}$$

where a_{ignition} was the strain rate at ignition and k_i was the reaction rate of the ith reaction. A positive sensitivity coefficient meant that increasing the reaction rate accelerated ignition and vice versa. Sensitivity analysis revealed that two reactions gained significant importance for ignition when the NO concentration was increased from 10,000 to 100,000 ppm. They were

$$NO_2 + O \rightarrow NO + O_2 \tag{15}$$

$$NO + O(+M) \rightarrow NO_2(+M) \tag{16}$$

A rate of production analysis for NO and NO_2 confirmed these results. Even though reactions (15) and (16) converted NO to NO_2 and vice versa, similar to the catalytic cycle, they consumed active atomic oxygen. Therefore, even though there was an order of

magnitude increase in NO addition, there was less relative ignition enhancement because NO and NO_2 reacted with active radicals, removing them from the ignition cycle. Furthermore, it was found that, regardless of the temperatures involved in the counterflow system, reactions (15) and (16) gained sensitivity with increased NO concentration, reaffirming what was identified in past works on ignition sensitivity to NO addition [26,27].

IV. Conclusions

The present study clearly identified the primary kinetic ignition enhancement mechanisms of counterflow diffusion flames by nonequilibrium plasma. The nonequilibrium MGA plasma discharge of air in a counterflow diffusion flame burner using CH_4–air and H_2–air resulted in significant kinetic ignition enhancement. Experimental measurements and computational simulations showed NO_x to be the primary means of ignition enhancement by plasma discharge of the air. However, the small differences shown between the plasma experimental results and computational results do not unequivocally block the idea of additional mechanisms of enhancement from plasma-produced species to affect ignition. Computational simulations reaffirmed that large concentrations of NO led to less relative ignition enhancement, showing that there was a critical concentration of NO which yielded the most efficient enhancement. Most importantly, the simulations showed the existence of two ignition regimes for low concentrations of NO addition (1000 ppm of NO), but three ignition regimes for higher concentrations of NO addition (10,000 ppm of NO). The ignition regimes were dependent upon the competition between the radical production by the catalytic effect of NO_x and other oxidation pathways, as well as heat release from exothermic reactions and thermal feedback to reach the critical branching factors required for ignition. The identification of the existence of different ignition regimes and critical concentrations of NO_x presents a new strategy for plasma-assisted ignition in supersonic flow. The strategy states that, depending upon the flow strain rate and concentration of plasma-produced NO_x, cold nonequilibrium plasma may not be the best choice for efficient ignition enhancement. A combination of thermal-equilibrium plasma, to raise the translational temperature of the gas and sustain species concentrations, and nonthermal/nonequilibrium plasma, to produce NO_x and active radicals, can yield optimal ignition enhancement results.

Acknowledgments

The authors would like to thank the Air Force Office of Scientific Research for supporting this work with grant number F49550-04-1-0038 under program manager, Julian Tishkoff, as well as to thank Kenichi Takita for support through a grant from the New Energy and Technology Development Organization. The authors also wish to thank Marcos Chaos and Michael Burke for their insightful discussions and help with some of the numerical work, as well as Skip Williams and Campbell Carter for their stimulating conversations.

References

[1] Brande, W. T., "Bakerian Lecture: On Some New Electro-Chemical Phenomena," *Philosophical Transactions of the Royal Society of London*, Vol. 104, 1814, pp. 51–61. doi:10.1098/rstl.1814.0005

[2] Kimura, I., Aoki, H., and Kato, M., "Use of a Plasma Jet for Flame Stabilization and Promotion of Combustion in Supersonic Flows," *Combustion and Flame*, Vol. 42, No. 3, 1981, pp. 297–305. doi:10.1016/0010-2180(81)90164-4

[3] Wagner, T. C., O'Brien, W. F., Northam, G. B., and Eggers, J. M., "Plasma Torch Igniters for Scramjets," *Journal of Propulsion and Power*, Vol. 5, No. 5, 1989, pp. 548–554. doi:10.2514/3.23188

[4] Barbi, E., Mahan, J. R., O'Brien, W. F., and Wagner, T. C., "Operating Characteristics of Hydrogen-Argon Plasma Torch for Supersonic Combustion Applications," *Journal of Propulsion and Power*, Vol. 5, No. 2, 1989, pp. 129–133. doi:10.2514/3.23126

[5] Takita, K., Murakami, K., Nakane, H., and Masuya, G., "Novel Design of a Plasma Jet Torch Igniter in a Scramjet Combustor," *Proceedings of the Thirtieth International Symposium on Combustion*, Combustion Inst., Pittsburgh, PA, 2005, pp. 2843–2849. doi:10.1016/j.proci.2004.08.110

[6] Esakov, I. I., Grachev, L. P., Khodataev, K. V., Vinogradov, V. A., and Van Wie, D. M., "Propane–Air Mixture Combustion Assisted by MW Discharge in a Speedy Airflow," *IEEE Transactions on Plasma Science*, Vol. 34, No. 6, 2006, pp. 2497–2506. doi:10.1109/TPS.2006.886090

[7] Stockman, E., Zaidi, S., and Miles, R., "Pulsed Microwave Enhancement of Laminar and Turbulent Hydrocarbon Flames," *45th AIAA Aerospace Sciences Meeting and Exhibit*, AIAA Paper 2007-1348, Jan. 2007.

[8] Chintala, N., Meyer, R., Hicks, A., Bao, A., William, R. J., Lempert, W. R., and Adamovich, I. V., "Nonthermal Ignition of Premixed Hydrocarbon-Air Flows by Nonequilibrium Radio Frequency Plasma," *Journal of Propulsion and Power*, Vol. 21, No. 4, 2005, pp. 583–590. doi:10.2514/1.10865

[9] Starikovskii, A. Y., Anikin, N. B., Kosarev, I. N., Mintoussov, E. I., Starikovskaia, S. M., and Zhukov, V. R., "Plasma-Assisted Combustion," *Pure and Applied Chemistry*, Vol. 78, No. 6, 2006, pp. 1265–1298. doi:10.1351/pac200678061265

[10] Pancheshnyi, S. V., Lacoste, D. A., Bourdon, A., and Laux, C. O., "Ignition of Propane-Air Mixtures by Repetitively Pulsed Nanosecond Discharge," *IEEE Transactions on Plasma Science*, Vol. 34, No. 6, 2006, pp. 2478–2487. doi:10.1109/TPS.2006.876421

[11] Bao, A., Utkin, Y., Keshav, S., and Adamovich, I., "Methanol and Ethanol Ignition by Repetitively Pulsed, Nanosecond Pulse Duration Plasma," *45th AIAA Aerospace Sciences Meeting and Exhibit*, AIAA Paper 2007-1387, Jan. 2007.

[12] Kim, W., Mungal, M. G., and Cappelli, M. A., "Flame Stabilization Using a Plasma Discharge in a Lifted Jet Flame," *43rd AIAA Aerospace Sciences Meeting and Exhibit*, AIAA 2005-931, 2005.

[13] Ombrello, T, Qin, X., Ju, Y., Gutsol, A., Fridman, A., and Carter, C., "Combustion Enhancement via Stabilized Piecewise Non-Equilibrium Gliding Arc Plasma Discharge," *AIAA Journal*, Vol. 44, No. 1, 2006, pp. 142–150. doi:10.2514/1.17018

[14] Takita, K., and Ju, Y., "Effect of Radical Addition on Extinction Limits of H_2 and CH_4 Flames," *44th AIAA Aerospace Sciences Meeting and Exhibit*, AIAA, 2006-1029, Jan. 2006.

[15] Kuznetsova, I. V., Kalashnikov, A. F., Gutsol, A. F., Fridman, A. A., and Kennedy, L. A., "Effect of 'Overshooting' in the Transitional Regimes of the Low-Current Gliding Arc Discharge," *Journal of Applied Physics*, Vol. 92, No. 8, Oct. 2002, pp. 4231–4237. doi:10.1063/1.1505682

[16] Ombrello, T., Qin, X., Ju, Y., Gangoli, S., Gutsol, A., and Fridman, A., "Non-Equilibrium Plasma Discharge: Characterization and Effect on Ignition," *44th AIAA Aerospace Sciences Meeting and Exhibit*, AIAA Paper 2006-1214, Jan. 006.

[17] Fotache, C. G., Kreutz, T. G., and Law, C. K., "Ignition of Counterflowing Methane Versus Heated Air Under Reduced and Elevated Pressures," *Combustion and Flame*, Vol. 108, No. 4, 1997, pp. 442–470. doi:10.1016/S0010-2180(97)81404-6

[18] Ju, Y., Guo, H., Maruta, K., and Liu, F., "On the Extinction Limit and Flammability Limit of Non-Adiabatic Stretched Methane-Air Premixed Flames," *Journal of Fluid Mechanics*, Vol. 342, July 1997, pp. 315–334. doi:10.1017/S0022112097005636

[19] Bowman, C. T., Hanson, R. K., Davidson, D. F., Gardiner, W. C. Jr., Lissianski, V., Smith, G. P., Golden, D. M., Frenklach, M., and Goldenberg, M., GRI-2.11 Mechanism [online], http://www.me.berkeley.edu/gri_mech/ [retrieved 16 Jan. 2007].

[20] Smith, G.P., Golden, D.M., Frenklach, M., Moriarty, N. W., Eiteneer, B., Goldenberg, M., Bowman, C. T., Hanson, R. K., Song, S., Gardiner, W. C., Jr., Lissianski, V. V., and Qin, Z., GRI-3.0 Mechanism [online] http://www.me.berkeley.edu/gri_mech/ [retrieved 12 February 2008].

[21] Li, J., Zhao, Z., Kazakov, A., and Dryer, F. L., "Updated Comprehensive Kinetic Model of Hydrogen Combustion," *International Journal of Chemical Kinetics*, Vol. 36, No. 10, 2004, pp. 566–575. doi:10.1002/kin.10168

[22] Mueller, M. A., Yetter, R. A., and Dryer, F. L., "Kinetic Modeling of the $CO/H_2O/O_2/NO/SO_2$ System: Implications for High-Pressure Fall-

Off in the $SO_2 + O(+M) = SO_3(+M)$ Reaction," *International Journal of Chemical Kinetics*, Vol. 32, No. 6, 2000, pp. 317–339. doi:10.1002/(SICI)1097-4601(2000)32:6<317::AID-KIN1>3.0.-CO;2-L

[23] Liu, W., and Law, C. K., "On Multiple Criticality in Hydrocarbon Ignition," *45th AIAA Aerospace Sciences Meeting and Exhibit*, AIAA Paper 2007-1425, Jan. 2007.

[24] Ombrello, T., Ju, Y., Gangoli, S., Gutsol, A., and Fridman, A., "Ignition Enhancement Using Magnetic Gliding Arc," *45th AIAA Aerospace Sciences Meeting and Exhibit*, AIAA Paper 2007-1025, Jan. 2007.

[25] Amano, T., and Dryer, F. L., "Effect of Dimethyl Ether, NO_x, and Ethane on CH_4 Oxidation: High Pressure, Intermediate-Temperature Experiments and Modeling," *Proceedings of the 27th International Symposium on Combustion*, Vol. 27, Combustion Inst., Pittsburgh, PA, 1998, pp. 397–404.

[26] Tan, Y., Fotache, C., and Law, C. K., "Effects of NO on the Ignition of Hydrogen and Hydrocarbons by Heated Counterflowing Air," *Combustion and Flame*, Vol. 119, No. 3, 1999, pp. 346–355. doi:10.1016/S0010-2180(99)00064-4

[27] Bromly, J. H., Barnes, F. J., Muris, S., You, X., and Haynes, B. S., "Kinetic and Thermodynamic Sensitivity Analysis of the NO-Sensitized Oxidation of Methane," *Combustion Science and Technology*, Vol. 115, Nos. 4–6, 1996, pp. 259–296. doi:10.1080/00102209608935532

J. Gore
Associate Editor